13th International Brick and
Block Masonry Conference
Amsterdam, July 4-7, 2004

ON THE CYCLIC BEHAVIOUR OF STONE DRY MASONRY JOINTS

Paulo B. Lourenço [1], **Luís F. Ramos**[2], **Graça Vasconcelos**[3]

Abstract

Dry masonry mechanics received little attention from research community, when compared with resources invested in traditional (mortared joint) masonry. Therefore, this work focuses on the characterization of Coulomb failure criterion and the load-displacement behaviour of dry masonry joints under cyclic loading, including aspects as surface roughness, dilatancy, inelastic behaviour, different stones and moisture contents. A displacement controlled test set-up using masonry couplets is used for this purpose. Besides providing a basis for understanding the behaviour of masonry joints, the experiments contribute also to the definition of non-linear numeric models.

Key Words

Masonry; Testing; Coulomb failure criterion; Cyclic loading.

1 Introduction

There is an important legacy of significant ancient constructions originally built with dry joint masonry, including the majority of the built stone heritage in the Near East, most blocky structures in Greece (such as the Parthenon), several Roman monuments (such as the famous Aqueduct in Segovia, Spain, or the Pont du Gard, France) or certain Medieval monasteries built in the south of Europe. On the other hand, several ancient constructions built with mortar joints, have experienced a significant loss of mortar due to environmental erosion and have become mechanically similar to constructions originally built with dry joints.

The present paper aims at contributing to improve the knowledge of dry joint masonry under cyclic shear loading, which is of crucial importance for seismic actions. The failure behaviour of masonry joints under shear, with moderate pre-compression levels, can be represented by the Coulomb friction law, which establishes a linear relationship between the shear stress τ and the normal stress σ, being given by:

$$\tau = c + \tan\phi \cdot \sigma \qquad (1)$$

[1] P.B. Lourenço, University of Minho, pbl@civil.uminho.pt, www.uminho.pt/masonry
[2] L.F. Ramos, University of Minho, ramos@civil.uminho.pt
[3] G. Vasconcelos, University of Minho, graca@civil.uminho.pt

Here, c represents the cohesion, which in the case of dry masonry joints assumes the value zero, and $\tan\phi$ is the tangent of the friction angle of the contact surface. For higher normal compressive stresses, the validity of the Coulomb failure is lost and crushing / shearing of the units, accompanied by diagonal cracking is found. In this case, a cap model can be adopted to represent failure of the combined joint-unit ensemble, see for example Lourenço and Rots (1997). Another relevant feature of masonry joints is the so-called dilatancy angle ψ, which measures the volume change upon shearing. The ratio between the normal displacement and the shear displacement gives $\tan\psi$, which can assume positive or negative values. Usually, the dilatancy angle is positive but tends to zero upon increasing shear displacement and increasing normal confining stress, see van der Pluijm (1999).
For the purpose of characterizing the Coulomb failure criterion, different test methods to determine the strength parameters c, $\tan\phi$ and the volume parameter $\tan\psi$ have been adopted by researchers (e.g. Copeland and Saxer, 1964; Hamid et al., 1979; Atkinson et al. 1989; and van der Pluijm, 1999). All test methods fail to reproduce an absolutely uniform distribution of the normal and shear stresses even if the triplet test has been adopted as the standard test in Europe, CEN (1995). The triplet test is rather complex to understand because it includes two joints that fail at different stages, see Lourenço et al. (2004a) for a discussion. Therefore, the testing method adopted here is the couplet test, with clamping devices such that the test set-up becomes rather similar to the well-known shear boxes, see Lourenço and Ramos (2004b) for details.
In the present paper, two different types of stones have been used for comparison (sandstone and granite). The testing equipment is able to follow the complete stress-displacement diagram, which allows for a full characterization of the most relevant friction features. Additionally, the stone surface was treated with different mechanical techniques so that polished, sawn and rough surfaces could be obtained. Finally, also the effect of moisture conditions has been assessed. This is a key issue for historical constructions as the masonry courses close to the foundations are often saturated.

2 Testing procedures

2.1 Materials

Two different stones have been considered for testing, namely Spanish “Montjuic” sandstone, widely used for the monuments in Catalonia, Spain, and Portuguese “Mondim de Basto” granite, widely used for the monuments in the North of Portugal. The dimensions of the specimens are $80 \times 50 \times 40$ mm^3.
The sandstone adopted for the tests is a sedimentary homogeneous stone with a soft texture and small grains (dimensions between 40 and 650 μm). The mechanical properties of this stone have been studied in detail by Oliveira (2003), which indicated a Young modulus of 18800 N/mm^2, a Poisson ratio of 0.3 and strength of 91.6 N/mm^2.
The granite adopted for the tests is an eruptive homogeneous stone with two mica and medium grain, see Vasconcelos et al. (2004) for a detailed description.

2.2 Test set-up and procedures

The tests were carried out in a specially developed CS 7400-S – Shear Testing System – from James Cox, which features two independent actuators: a vertical actuator associated with the normal stress and a horizontal actuator associated with the shear stress. Each actuator has a maximum load capacity of ±20 kN, both in tension and compression. Besides the internal displacement transducers of each actuator, three Linear Variable Displacement Transducers (LVDTs) were located at the face of the specimens, see Figure 1a. The normal stress given by F_n was kept constant and equal to three compressive normal stress levels (0.5, 1.0 and 1.5 N/mm^2), see Figure 1b. After the application of this confining stress, the shear displacement δ_s was applied at a

constant rate of ±2.5 mm/s. As the normal stress was kept constant, the specimens were free to move in the vertical direction due to dilatancy effects.

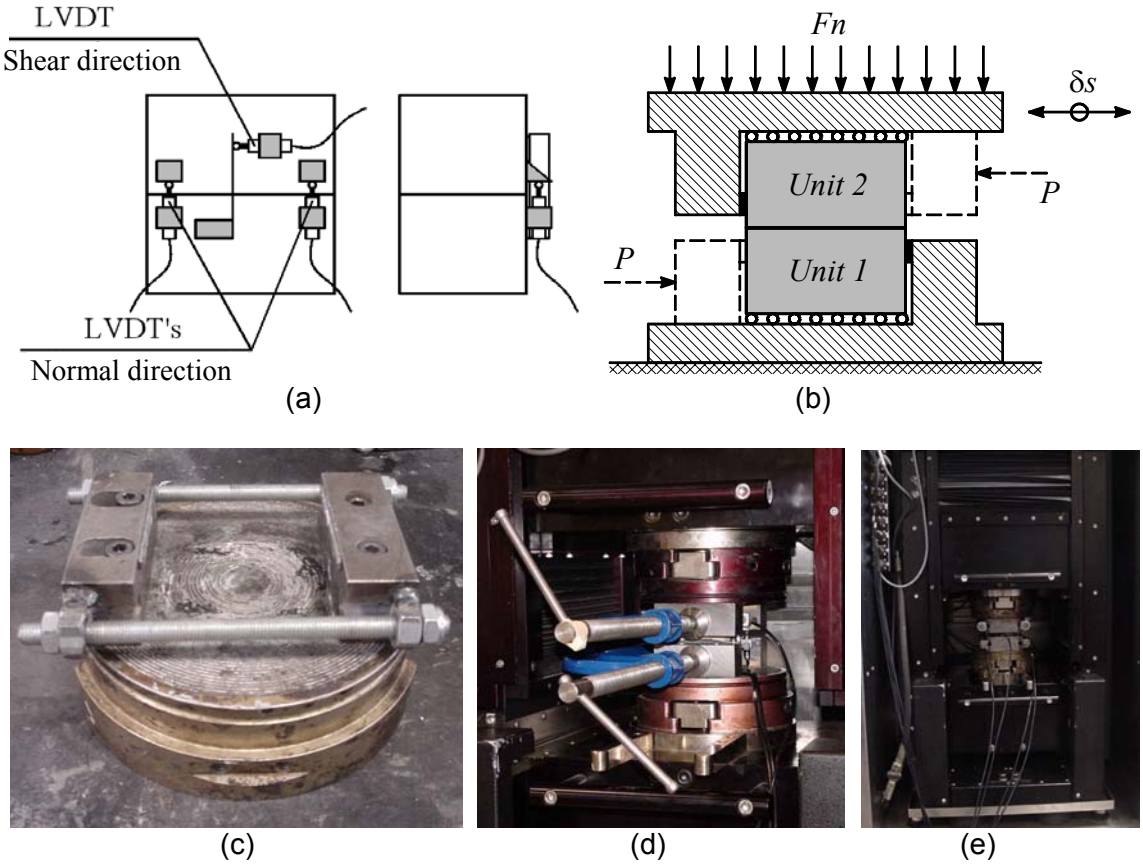

Figure 1 Details of test set-up: (a) location of the external LVDTs; (b) force and displacement imposed to the specimen; (c) detail of steel platens and steel clamps; (d) levelling of epoxy layer; (e) CS 7400-S testing equipment

The tests specimens were placed in circular steel platens that were clamped to the actuators, so that rotations of the platens were not allowed. The specimens are made of two independent stone units and, therefore, each single unit was fixed to one steel platen, using additional clamps fastened to the steel platens with two bolts. It is noted that one of the clamps was provided with oval openings in order to allow for adequate adjustment of the stone unit to the platen, Figure 1c.

The contact of the clamps with the stone units was made using two neoprene shims. In addition, two lubricated Teflon layers were placed between the stone units and the steel platens. The usage of the neoprene shims ensures that the shear load is applied in the neighbourhood of the joint and the usage of Teflon layers ensures that no friction is present between the stone units and the platens, which is of relevance for load-reversal. Due to the displacement inversion during testing, a small pre-compression of the stone units along the horizontal direction has been applied.

The process for preparation of the specimens can be described as follows:

1. Teflon layers were pre-placed on the machine platens;
2. A layer of epoxy resin (DEVCON) was applied between the stone unit and the Teflon contacting layer. The thickness of this layer was 3 mm and the objective was to ensure perfectly levelled surfaces, even if the stone units had been properly sawn and ground in the face contacting the Teflon layers;
3. The rubber shims were placed close to the edges of the stone units and the prisms were confined with the clamps;

4. Both platens were clamped and the pre-compression was applied and kept constant for approximately one hour, so that the epoxy resin could be perfectly levelled, see Figure 1d. Specimens ready for testing, see Figure 1e.

2.3 Validation of test set-up

To validate the test set-up, a finite element model was built, including eight-noded continuum elements to represent the steel clamps, the neoprene shims and the stone units, and six-noded zero thickness interface elements to represent the joint. The inelastic behaviour of the interface has been modelled at this evaluation stage using an ideal-plastic Coulomb friction law, with zero cohesion and a friction angle given by $\tan\phi$ equal to 0.75.

Figure 2a presents the stress distribution in the joint at ultimate stage (maximum load) for monotonic loading, which is obviously non-uniform. The peaks of the normal stresses are perfectly correlated with the peaks of the shear stresses, as it should be expected due to the Coulomb failure criterion. Figure 2b indicates that all the integration points are aligned with the failure criterion, but with different normal stress levels. The average normal stress value stays equal to 1.0 N/mm^2, with a peak value of 1.43 N/mm^2. The average shear stress is equal to 0.75 N/mm^2. This means that the ratio between the shear and normal average stresses is equal to the value adopted for input of the failure criterion, i.e. $\tan\phi = 0.75$, which allows concluding that the proposed test set-up is adequate for the purpose of identifying the mechanical data for the Coulomb failure criterion. It is also noted that the distribution of the normal and the shear stresses is almost constant for more than 60% of the length of the joint.

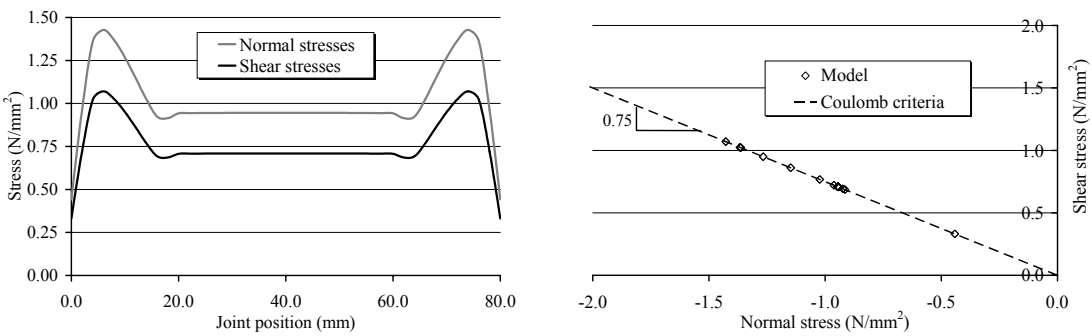

(a) (b)

Figure 2 Distribution of stresses in the joint after sliding: (a) normal and shear stresses; and (b) location of integration points with respect to the Coulomb failure criterion

3 Test results for sandstone

The study using sandstone contemplated three different types of treatments for the stone surface, namely: (a) polished surface using sandpaper number 180 (specimens denoted as P series); (b) mechanically sawn surface (specimens denoted as S series); and (c) artificially rough surface using a mechanically random spike (specimens denoted as R series). With the proposed approach it is possible to compare the influence of the stone surface roughness in the behaviour of the dry joints.

The key mechanical parameter of the dry joints is $\tan\phi$, which can be obtained by linear regression from tests with different normal confining stresses. Here, three levels of normal stress have been considered, namely 0.5, 1.0 and 1.5 N/mm^2. For each stress level and each surface treatment, three identical specimens have been tested, making a total of twenty-seven specimens, see also Lourenço and Ramos (2004b).

The tests were carried out under displacement control, using the horizontal LVDT positioned in the direction of the shear load. The histogram of imposed horizontal

displacements was defined according to the surface treatment, from preliminary tests. From the behaviour observed in preliminary tests, the following loading cycles have been adopted: (a) P series – six loading cycles with ±0.1 / ±0.2 / ±0.3 / ±0.4 / ±0.4 / ±0.4 mm; (b) S series – four loading cycles with ±0.1 / ±0.2 / ±0.3 / ±0.4 mm; (b) R series – seven loading cycles with ±0.1 / ±0.2 / ±0.3 / ±0.4 / ±0.8 / ±1.2 / ±1.6 mm.

3.1 Load-displacement diagrams

The typical behaviour of the specimens for series P (polished surface) is given in Figure 3a. It can be observed that the elastic behaviour is followed by fully plastic behaviour, as no recover of the joint deformation occurred upon load removal. The (small) shear strength increase with plastic deformation and the (considerable) shear strength increase with the loading cycles was unexpected. This behaviour occurred for all specimens, independently of the level of vertical confining stress. It is believed that the increase of the shear strength can be justified by the roughness increase of the stone surface upon shearing and, consequent, wearing of the joint. After completing the loading / unloading cycles, wearing of the stone surface was encountered in all specimens.

The typical behaviour of the specimens for series S (sawn surface) is given in Figure 3b. For this series, the presence of a non-linear branch in the pre-sliding phase is clearly visible. This non-linear branch, which indicates progressive sliding of the joint and simulates stiffness degradation of the dry joints, is not found in the unloading branches. It is also observed that the shear strength remains constant with an increasing number of loading cycles. The slightly lower shear strength for the first cycle indicates that the final displacement of the first cycle was insufficient to reach the maximum shear strength. In the specimens tested with lower vertical confining stress, no difference was found between the shear strength of the first loading branch and the additional cycles.

The typical behaviour of the specimens for series R (rough surface) is given in Figure 3c. For this series, the presence of a non-linear branch in the pre-sliding phase is also clearly visible. Again, this non-linear branch is not found in the unloading branches. The shear strength increases during the first three / four cycles but then remains constant with an increasing number of loading cycles. This phenomenon is most likely related to the wearing of the interlocking localized contacts between the rough surfaces. Finally, it is also noted that non-symmetric behaviour and hardening during plastic shearing were found, which are attributed to the randomness of contact in the artificially, mechanically produced, rough surface.

3.2 Coulomb failure criteria

Coulomb friction law fits very well the experiments, with an average linear regression factor r^2 equal to 0.96, upon enforcing zero cohesion.

The failure criteria obtained for the three series of stone specimens were different for the initial values (first cycle) and for the final values (last cycle). The results in terms of $\tan\phi$ vary also significantly according to the surface treatment and upon wearing of the surface, see Table 1.

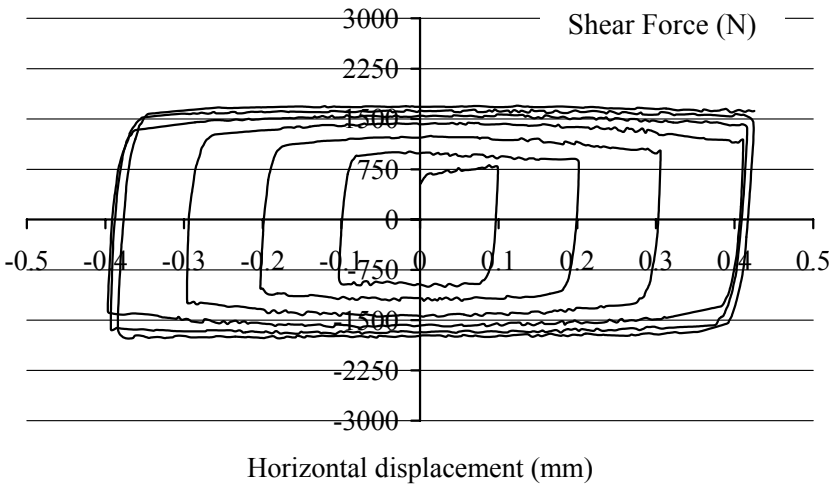

(a)

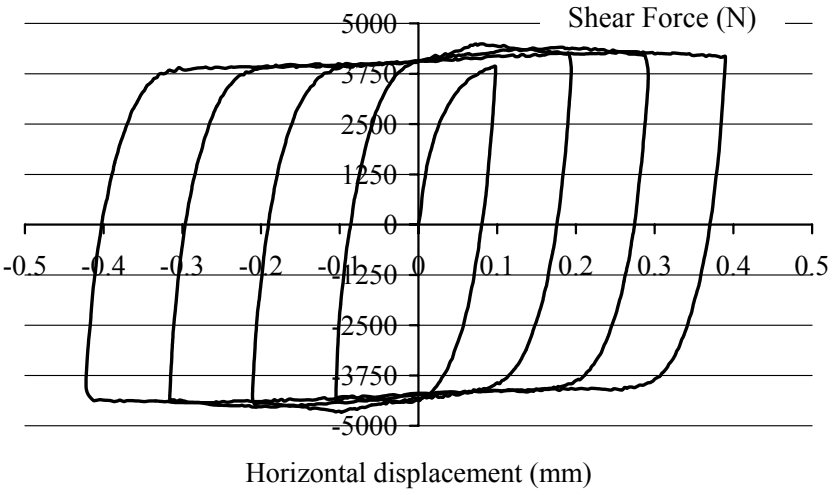

(b)

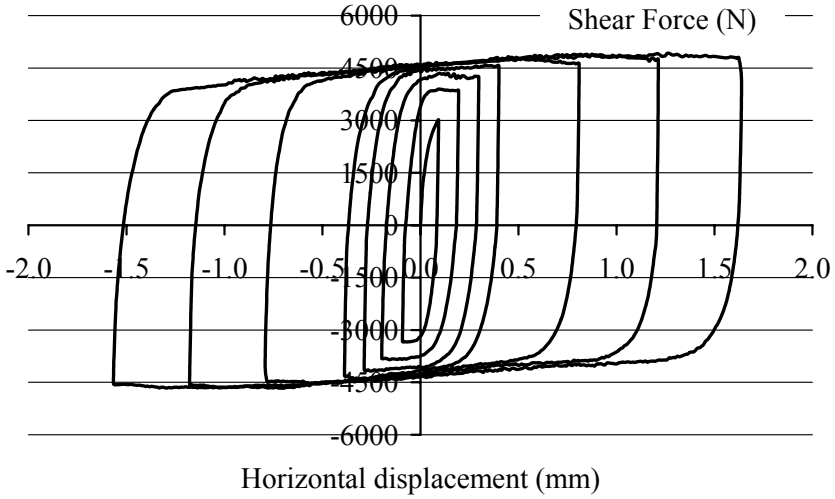

(c)

Figure 3 Typical load-displacement diagrams for a pre-confining level of 1.5 N/mm^2: (a) Series P; (b) Series S; (c) Series R

Table 1 Tangent of the friction angle for the different series.

Series	$\tan\phi_i$	$\tan\phi_f$	$\tan\phi_i / \tan\phi_f$
P (Polished)	0.18	0.43	2.4
S (Sawn)	0.62	0.63	1.0
R (Rough)	0.56	0.74	1.3

Series P exhibits a low initial friction angle ($\tan\phi_i$ = 0.18) due to the smoothness of the surface and a very significant difference between the initial and the final friction angle ($\tan\phi_f$ / $\tan\phi_i$ = 2.4). Series S exhibits no variation between the initial and final friction angle, which seems characteristic of sawn specimens (see also Section 4.1), meaning that sawn surfaces have a roughness similar to the surfaces obtained by a stone wearing process. Finally, series R exhibits an initial friction angle lower than series S but upon wearing the values increase, as expected, to the highest value of all series. Therefore, it seems possible to state that an increase of the surface roughness, results in an increase of the final friction angle.

3.3 Dilatancy

The dilatancy angle ψ measured in all series was very low (lower than ±0.05) and a value of zero is recommended, see Figure 4a. Nevertheless, series R exhibits a significant localized reduction of volume upon load reversal, see Figure 4b, even if inside each cycle the value of the $\tan\psi$ remains very low. This phenomenon, which is again associated with wearing of the contact points between the rough surfaces, does not occur in series P and S. The value of the total vertical compaction of the specimens was, on the average, equal to 0.4 mm. The rate of compaction decreases with increasing cycles and an "equivalent" dilatancy angle ψ^* can be defined as the ratio between vertical compaction and total displacement per cycle. In this case, the initial value for $\tan\psi^*$ is equal to –0.3 and a final value is equal to –0.01.

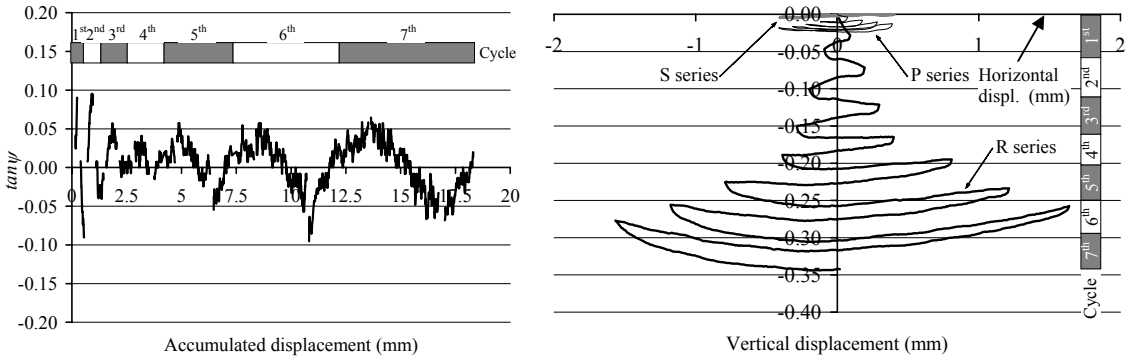

(a) (b)

Figure 4 Volume changes: (a) typical variation of the dilatancy angle; and (b) relation between horizontal and vertical displacements for all series

3.4 Pre-peak inelastic behaviour

The variation of stiffness in the pre-peak phase is significant, as illustrated by means of a shear force vs. horizontal displacement diagram in which the elastic horizontal displacement of the stone itself is removed from the total displacement. The joint horizontal displacement u_{joint} is then given by

$$u_{joint} = u_{measured} - \frac{\tau}{k_{shear}} \tag{2}$$

where $u_{measured}$ is the value read in the LVDT and the shear stiffness k_{shear} is calculated from the unloading branches, dividing the variation of shear stress Δ_t up to zero by the

respective variation of the shear displacement $\Delta u_{measured}$. The values of the shear stiffness obtained are constant through cycles, which indicate linear elastic behaviour of the stone. It is observed that the unloading branches are vertical, which represents fully plastic behaviour of the joint upon load removal, but the reloading branches exhibit gradual inelastic behaviour (or hardening behaviour). The existence of a variable stiffness of the dry joint indicates progressive sliding of the joint and cannot be associated with an elastic (recoverable) continuum deformation.
The global behaviour of all the joints seems to be illustrated adequately using the load-displacement diagram and failure criterion indicated in Figure 5. The branches with the letter *a* indicate hardening behaviour, after which ideal plastic behaviour follows (branches indicated by the letter *b*). The unloading stage is identified with the letter c, which represents full plastic behaviour of the joint or, equivalently, infinite unloading stiffness. The changes in the hardening behaviour are not significant and, for practical purposes, the different branches a_1, a_2, …, a_f can be considered equal and independent from the loading cycle. On the contrary, the experimental results indicate that the shape of the hardening branch *a* depends on the applied normal stress level.

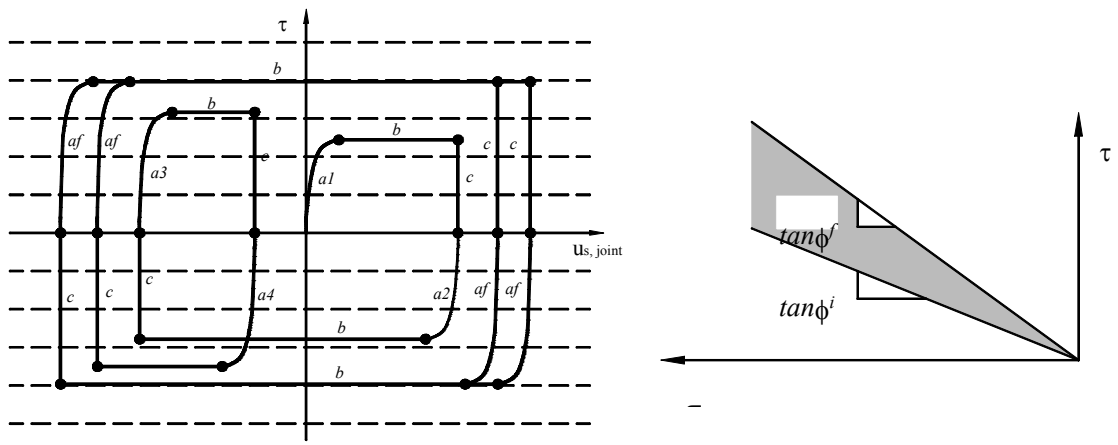

Figure 5 Typical observed behaviour of dry joints: (a) hysteretic diagram; and (b) failure criterion

4 Test results for granite

The study using granite contemplated only the mechanically sawn surface but the influence of the water contents is also addressed. This is a key issue for historical buildings, which usually have very high moisture conditions.
Again, three levels of normal stress have been considered, with three specimens for each stress level, in a total of 18 specimens. The test results for granite are similar to the results for sandstone, with respect to load-displacement diagrams, dilatancy and pre-peak inelastic behaviour, so they will not be given here. Only the Coulomb failure criteria and the influence of the moisture will be addressed.

4.1 Coulomb failure criteria

Coulomb friction law fits very well the experiments, with an average linear regression factor r^2 equal to 0.99, upon enforcing zero cohesion. The value obtained for the friction angle is 0.64 (both for initial and final values), meaning that the value for the selected sandstone and granite are the same.

4.2 Influence of moisture conditions

All previous tests have been carried out for stone in air-dry conditions. In addition, fully saturated tests have also been carried out at this stage. Coulomb friction law fits again

very well the fully saturated experiments, with an average linear regression factor r^2 equal to 0.96, upon enforcing zero cohesion. The value obtained for the (saturated) friction angle is 0.61, meaning that the influence of moisture conditions are negligible for practical purposes. This is hardly the case for tensile or compressive strengths, where the results are strongly dependent on moisture conditions, see e.g. Vasconcelos et al. (2004).

5 Conclusions

This paper addresses the issue of the behaviour of dry masonry joints. Deformation controlled couplet tests are used for this purpose. Two types of stone have been selected, namely sandstone (widely used in Spanish monuments) and granite (widely used in Portuguese monuments).

The following conclusions can be made from the tests:

1. No recover of the joint shear displacement occurred upon load removal, meaning that fully plastic deformation remains upon load removal. Hardening has been found in the loading regime, which indicates progressive sliding of the dry joint and cannot be associated with recoverable continuum deformation;
2. Coulomb friction law fits very well the experiments;
3. Polished stone surfaces exhibit a very low initial friction angle. Upon wearing due to cyclic loading, a continuous increase of the friction angle is found;
4. Sawn stone surfaces exhibit initial friction angle equal to 0.63-0.64, both for the sandstone and the granite tested. The different between the initial and the final friction angle is, in this case, marginal;
5. Irregular surfaces exhibit an initial friction angle lower than sawn surfaces but upon wearing the friction angle increases to the highest value of all series. Therefore, an increase of the surface roughness, results in an increase of the final friction angle;
6. The dilatancy angle measured in all series was very low (lower than ±0.05) and a value of zero is recommended fro practical purposes. For irregular surfaces, an equivalent negative dilatancy angle has been found;
7. Moisture conditions have marginal influence in the values of the friction angle of dry stone joints.

References

Atkinson, R.H., Amadei, B.P., Saeb, S., Sture, S., 1989, Response of masonry and joints in direct shear, J. Struct. Engrg, ASCE, 115(9), 2276-2296.

CEN – European Committee for Normalization, 1995, Methods of Test for Masonry; Determination of Initial Shear Strength, prEN 1052. Part 3

Copeland, R.E., Saxer, E.L., 1964, Tests on structural bond of masonry mortars to concrete block, J. Amer. Conc., Inst., 61(11), 1411-1451.

Hamid, A.A., Drysdale, R.G., Heidebrecht, A.C., 1979, Shear strength of concrete masonry joints, J. Struct. Div., ASCE, 105, 1227-1240.

Lourenço, P.B., Rots, J.G., 1997, A multi-surface interface model for the analysis of masonry structures, J. Engrg. Mech., ASCE, 123(7), 660-668.

Lourenço, P.B., Barros, J.O., Oliveira, J.T., 2004a, Shear testing of stack bonded masonry, Construction and Building Materials , 18, 25-132.

Lourenço, P.B., Ramos, L.F., 2004b, Characterization of cyclic behaviour of dry masonry joints, J. Struct. Engrg., ASCE, 130(5).

Oliveira, D.V., 2003, Experimental and numerical analysis of blocky masonry structures under cyclic loading, PhD Thesis, University of Minho, Portugal. Available at www.civil.uminho.pt/masonry.

Pluijm, R. van der, 1999, Out of plane bending of masonry behaviour. PhD Thesis. Eindhoven University of Technology, The Netherlands.

Vasconcelos, G., Lourenço, P.B., Alves, C.A.S., Pamplona J., 2004, Experimental properties of granites, Proc. 6th Int. Symp. Conservation of Monuments in the Mediterranean Basin, Lisbon (accepted for publication).